2006

Shape-Persistent V-Shaped Mesogens-Formation of Nematic Phases with Biaxial Order

Matthias Lehmann
Shin-Woong Kang, *Kent State University - Kent Campus*
Christiane Köhn
Sönke Haseloh
Ute Kolb, et al.

Shape-persistent V-shaped mesogens—formation of nematic phases with biaxial order†

Matthias Lehmann,*[a] Shin-Woong Kang,[b] Christiane Köhn,[a] Sönke Haseloh,[c] Ute Kolb,[c] Dieter Schollmeyer,[d] QingBing Wang[b] and Satyendra Kumar[e]

Received 21st April 2006, Accepted 7th August 2006
First published as an Advance Article on the web 19th September 2006
DOI: 10.1039/b605718g

A homologous series of *shape-persistent V-shaped* molecules has been designed to form the biaxial nematic phase. Phenyleneethynylene moieties are attached to a bent fluorenone unit to create an apex angle of about 90°, which is determined from the single crystal structure. Two mesogens, one symmetric and another unsymmetric, have been synthesized by attaching a cyano group to one or both of the peripheral phenyl units, respectively. These groups introduce local dipoles essential for the formation of the nematic phases. The tendency to form a crystalline phase is reduced by laterally substituted hexyloxy chains which allow the nematic phase to be supercooled to a glassy state. Two of the three fluorenone derivatives exhibit a transition from the uniaxial nematic to the biaxial nematic phase. This transition has an undetectably small transition enthalpy, but the X-ray diffraction, polarizing optical microscopy, and conoscopy reveal the presence of the biaxial order in the low temperature nematic phase.

Introduction

Recently, V-shaped mesogens based on an oxazoline centre came into the limelight, because they exhibit[1] the ever so elusive biaxial nematic (N_b) liquid crystal phase. Since the prediction of its existence by Freiser[2] and the first verification of the biaxial nematic phase in a lyotropic system by Yu and Saupe,[3] many attempts have been made to synthesize biaxial nematogens. Most of the synthetic effort has focussed on board-shaped (or, sanidic) mesogens. Practically none of the claims, before 2002, of the discovery of the N_b phase in small molecule mesogens could be substantiated.[4] In addition to the synthesis and study of board-shaped mesogens in the hope of realizing the N_b phase, theoretical and experimental investigations of mixtures of disk- and rod-shaped mesogens, such as mesogenic oligomers and polymers, have also been undertaken.[5]

Recently discovered rigid V-shaped mesogens were considered as good candidates for the formation of the biaxial nematic phase due to their inherent molecular biaxiality. A number of theoretical and simulation studies investigated suitable geometric shapes and calculated the phase diagrams for such materials. Luckhurst[4a] and Masters *et al.*[6] predicted that nematogens with a tetrahedral angle (*i.e.*, ~109°) between the two arms of the V-shaped molecule were the most promising candidates. However, the thermotropic V-shaped mesogens forming the thermotropic N_b phase,[1,7] have apex angles of about 140° and 120°. The effect of a local dipole moment that these mesogens possess was not considered in the theoretical models and, as has been suggested,[8] may play an important role in the organisation of the mesogens and establishment of the biaxial order. In addition to the N_b phase, biaxial smectic[9] phases also have been reported in banana shaped non-symmetric mesogens with dipoles. Therefore, we envisage the new shape-persistent V-shaped mesogen **1** to be a good system[10] to study the dependence of the nature of resulting nematic phases on the molecular architecture. These mesogens are based on rigid oligophenyleneethynylene wings attached to different core units at various angles. The presence of alkoxy chains in the 2,5-position of the central benzene ring appears to favour the formation of nematic LC phases as evident from the study of stilbenoid oligomers[11] and polymers.[12] In these materials, local dipoles may be introduced at the central and peripheral aromatic units by electron-withdrawing substituents. Here, we present the synthesis and characterization of the phases formed by V-shaped mesogens with hexyloxy chains and a fluorenone core (**1a–c**). A model for their supramolecular self-assembly is proposed.

Results and discussion

Synthesis

An optimised strategy, shown in Scheme 1, was applied for the synthesis of unsymmetric phenyleneethynylene oligomers. The key precursor in the synthesis scheme is the 4-bromo-2,5-dihydroxyiodobenzene **3**.[13] After etherification with hexylbromide, unsymmetric compound **5** can be synthesised using a

[a]*Chemnitz University of Technology, Strasse der Nationen 62, 09111, Chemnitz, Germany. E-mail: Matthias.Lehmann@chemie.tu-chemnitz.de; Fax: (+) 49/371 531 1839; Tel: +49 371 531 1205*
[b]*Department of Physics, Kent State University, Kent, OH 44242, USA*
[c]*Institute of Physical Chemistry, Johannes Gutenberg-University Mainz, Welderweg 11, 55099 Mainz, Germany*
[d]*Institute of Organic Chemistry, Johannes Gutenberg-University Mainz, Duesbergweg 10-14, 55099 Mainz, Germany*
[e]*National Science Foundation, 4201 Wilson Blvd., Arlington, VA 22230, USA*

† Electronic supplementary information (ESI) available: Comparision of ^{13}C NMR data, X-ray of oriented samples, simulated powder pattern, view along the *c*-axis of the single crystal of **1a** with characteristic distances. See DOI: 10.1039/b605718g

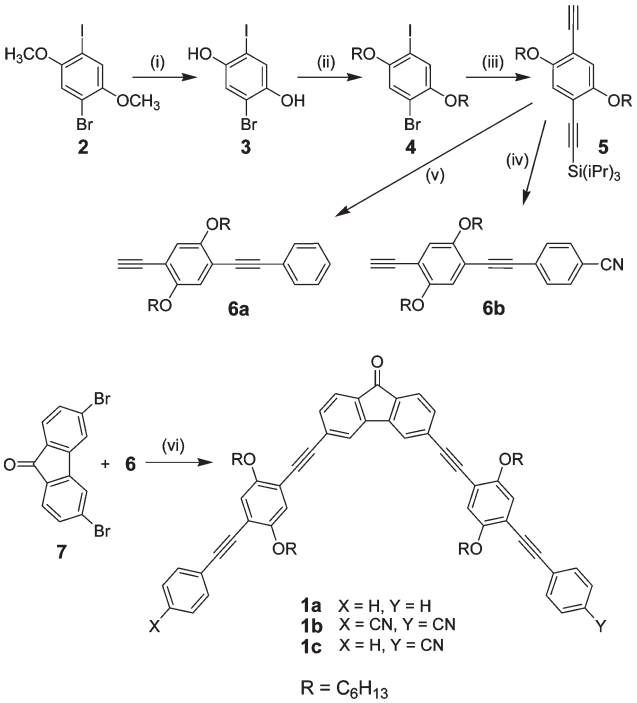

Scheme 1 Synthesis of V-shaped, shape-persistent mesogens **1**. *Reagents and conditions*: (i) BBr_3, CH_2Cl_2, 77%; (ii) KOH, DMF, $C_6H_{13}Br$, 82%; (iii) 1) piperidine, $Pd(PPh_3)_4$, CuI, $HC{\equiv}CSi(iPr)_3$; 2) $HC{\equiv}CSi(CH_3)_3$; 3) K_2CO_3, MeOH, THF, 92%; (iv) 1) piperidine, $Pd(PPh_3)_4$, CuI, PhI; 2) $(H_9C_4)_4NF$, THF, 81%; (v) 1) piperidine, $Pd(PPh_3)_4$, CuI, 4-bromobenzonitrile; 2) $(H_9C_4)_4NF$, THF, 77%; (vi) piperidine, $Pd(PPh_3)_4$, CuI, 33–52%.

one-pot reaction procedure,[10,14] followed by selective cleavage of the trimethylsilyl group. The peripheral aromatic units were cross-linked with **5** and the remaining protecting group was detached to yield the individual arms **6a,b**.[10] These arms have been coupled to the fluorenone dibromide **7**[15] to yield symmetrical V-shaped molecules **1a** and **1b**.[10] The non-C_2-symmetrical compound **1c** was prepared in a stoichiometric reaction with **6a** and **6b** (ESI†). The target molecules were fully characterised by NMR, FT-IR, mass spectroscopy and elemental analysis.

Molecular structure

A single crystal analysis of **1a** revealed the geometry of the rigid V-shaped mesogens.[16] Although the structure of the 3,6-disubstituted fluorenone core, which was energetically minimised by the semiempirical AM1 method, should have a bend angle θ of about 82°, it is found to be approximately 90° (Fig. 1) in the crystal phase. The rigid scaffold has a length of L = 24.3 Å and a width of B = 15.4 Å along the bisector. The fluorenone cores orient in anti-parallel manner and column-like stacks. Mesogens **1a–c** have different local terminal dipole moments. The keto group contributes to the dipole moment along the bisector of the molecule, whereas the cyano groups provide a dipole moment with components in opposite and orthogonal directions to the keto group. Using simple addition of local dipoles,[17] compound **1a** is estimated to have a dipole moment of approximately 3.38 D along the bisector which

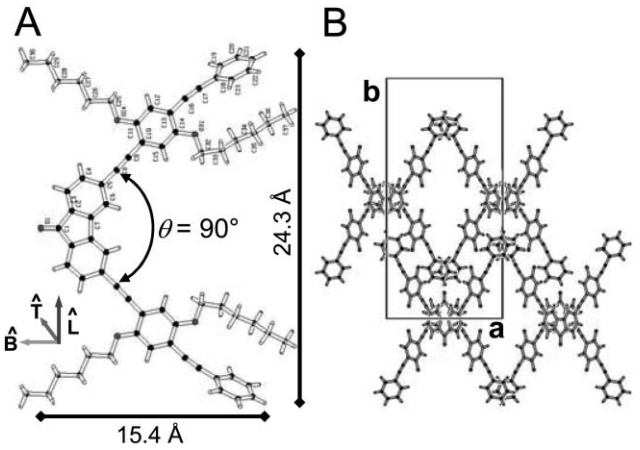

Fig. 1 X-Ray structure of **1a**, crystallised from acetone. The molecule lies with C1–O1 on a twofold axis. The molecular axes are defined as B (along the bisector), T (in the direction of normal of the fluorenone plane; thickness of the mesogen; which in the nematic phase is parallel to the director $\boldsymbol{n}$) and L (along the length of the molecule perpendicular to the bisector). B: The view along the c-axis. Molecules are aligned in an anti-parallel manner. The alkyl chains are omitted for clarity.

may be the driving force for the anti-parallel organisation of mesogens in the crystal phase. In compound **1b**, the net dipole moment (~2.35 D) parallel to the bisector is in the opposite direction due to the large contribution of the two cyano groups. However, the lateral components of the dipoles cancel because of the molecular C_{2v} symmetry. The situation is different in the case of the non-C_2-symmetric compound **1c**. Here, the single cyano group on one arm not only reduces the molecular dipole moment (to approx. 0.52 D) along the bisector, but also establishes a lateral component of ~2.86 D, which may favour the alignment of the second molecular axis (L).[9,18]

Thermotropic mesomorphic properties

The mesomorphic properties of these materials have been investigated by means of polarizing optical microscopy (POM), differential scanning calorimetry (DSC), and X-ray diffraction (XRD). Table 1 summarises the results. Derivative **1a**, without cyano substituents, does not possess mesomorphic properties. It only melts into the isotropic phase upon heating and then freezes into a glassy state when cooled. However, the other two mesogens **1b** and **1c** bearing cyano groups on the peripheral phenylene units, form nematic phases. Compound **1b** shows a stable, enantiotropic nematic phase above 161.3 °C,

Table 1 Mesomorphic properties of **1a–c**

Compound	DSC results from second heating at a rate of 10 °C min^{-1} (onset/°C; ΔH/kJ mol^{-1} [a])
1a	**g** 29.7 (T_g) **I** (melting at 104.3 °C)[b]
1b	**g** 34.4 (T_g) **N** 178.0/0.7 **I** (melting at 161.3 °C)[b]
1c	**g** 26.4 (T_g) **N** 121.8/0.4 **I** (melting at 132.3 °C)[b]

[a] **Cr** crystal, **g** glass, **N** nematic phase, **I** isotropic phase. [b] Phases reversibly observed at a heating rate of 10 °C min^{-1}. Annealing above the glass transition in the nematic or isotropic phases and below the given melting temperatures results in slow crystallisation.

but crystallizes slowly upon annealing at temperatures below 161.3 °C and above the glass transition. Mesogen **1c** exhibits only monotropic nematic phases. The transition enthalpies of 0.7 kJ mol^{-1} ($\Delta S/R$ = 0.19) for **1b** and 0.4 kJ mol^{-1} ($\Delta S/R$ = 0.11) for **1c**, provide evidence of the first order nature of the isotropic–nematic transition. The nematic phase of both compounds freezes to a nematic glass near room temperature (RT), which prevents crystallisation. This effect is attributed to the lateral attachment of short alkoxy chains. The side chains at 2,5-positions not only prevent facile crystallisation but also nanosegregation and thus make the formation of mesophases of higher supramolecular order (columnar or lamellar phases), which are often observed in conventional nematogens,[4] improbable. Therefore, this property should help the formation of the biaxial nematic phase at lower temperatures.

Optical textures and interesting electro-optical properties are observed in cells with a 10–15 μm gap prepared with untreated and ITO-coated glass substrates treated with two different polyimides. One of them is known to generate homogeneous, while the other produces homeotropic boundary conditions for calamitic mesogens. Surprisingly, surfaces with homeotropic anchoring conditions produce planar director orientation for these bent-core materials, while homogeneous surface conditions produce homeotropic alignment. In cells with homeotropic anchoring, sample **1c** shows a typical planar orientation with s = ½ (*i.e.*, 2-brush) disclinations, Fig. 2a,b, throughout the nematic temperature range. As the temperature is lowered below the clearing point in cells with *homogeneous* boundary conditions (and homeotropic alignment), the transition to the N_u phase appears *via* the formation of a typical but transient nematic Schlieren texture (Fig. 2c). The nematic director ***n*** (parallel to the molecular axis *T*; *cf.* next paragraph and Fig. 1) then immediately adopts a *homeotropic* orientation (Fig. 2d) and the sample appears dark between crossed polarizers. In this phase, rotation of the sample between crossed polarizers does not give rise to any variation in the intensity of transmitted light. Evidently, no optical anisotropy was present in the plane perpendicular to the director ***n***, pointing clearly to the uniaxial nature of this phase. The optical texture becomes gradually brighter below 80 °C as the birefringence associated with biaxiality develops in the plane perpendicular to the director ***n***. The cell is brightest when the rubbing direction, *R*, is at 45° with respect to the polarizer/analyzer axes (Fig. 2e). This marks the onset of the N_b phase and indicates that the secondary director ***m*** aligns along *R*, which we assume to be parallel to the axis *B*. The transmitted intensity is minimum when the rubbing direction is parallel to either the polarizer or the analyzer axis (Fig. 2f). The brightness of the texture continues to increase with increasing biaxial order at lower temperatures. The results of the optical retardation measurements made on a thin homogeneously aligned cell as a function of temperature are shown in Fig. 3. The measured retardation is proportional to the optical birefringence in the place of the cell. The data show a change in temperature dependence of the birefringence at the onset of biaxiality (ESI†[19] at 80 °C (Fig. 3) as is expected.

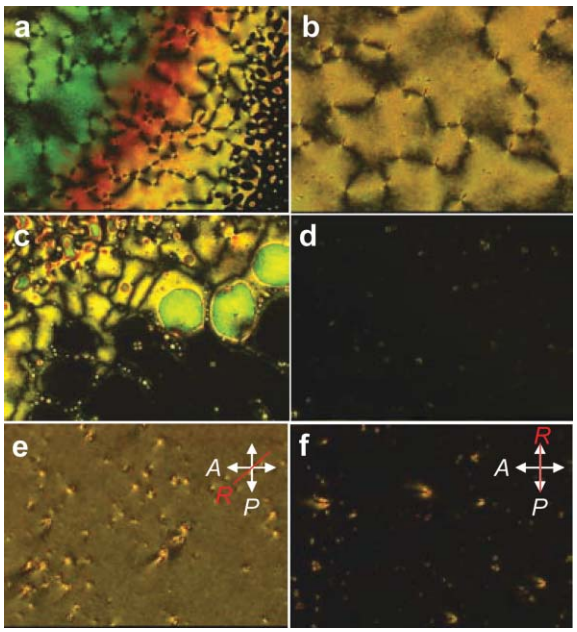

Fig. 2 POM textures of **1c** in a cell with homeotropic boundary conditions: (a) at the I to N_u transition and (b) at 50 °C. (c–f) Optical texture of sample **1c** in a cell with homogeneous boundary conditions. The rubbing direction *R* is at 45° to the polarizer and analyzer directions. (c) Schlieren texture (118.2 °C) near the I to N_u transition during cooling. (d) The N_u phase adopts homeotropic orientation for the director ***n***. (e) Birefringent texture of the N_b phase at 25 °C with ***n*** perpendicular to the cell and ***m*** most likely oriented along the rubbing direction, and (f) with ***m*** parallel to polarizer axis.

Conoscopy is a method that has traditionally been used to investigate the orientation of optic axes in a crystalline sample and is often used to infer the phase biaxiality. It requires well aligned single domain samples.[4,19,20] A systematic conoscopic study of a homeotropically aligned sample of **1c** was performed. The symmetric conoscopic cross shown in Fig. 4a in the nematic phase at high temperatures affirms its uniaxial nature. It practically remains unchanged from 120 °C down to approximately 75 °C in the N_u phase, below which it slowly evolves into the shape of a dagger and moves off-centre,

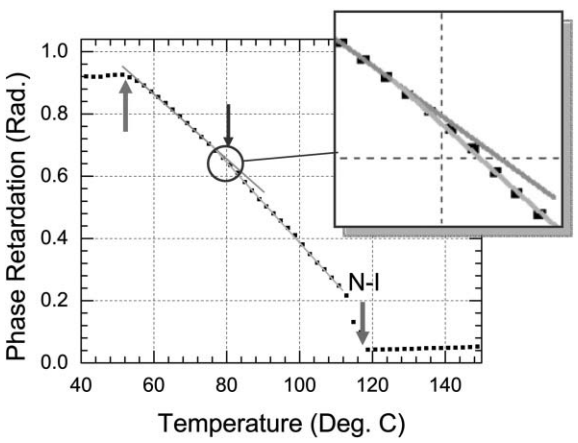

Fig. 3 Phase retardation ($\propto$ birefringence) of **1c** upon cooling from the isotropic phase. Arrows show temperatures with changes in the slope of the curve. The inset provides a magnified view of the data in the proximity of 80 °C. The slope changes at the onset of the biaxial nematic phase.

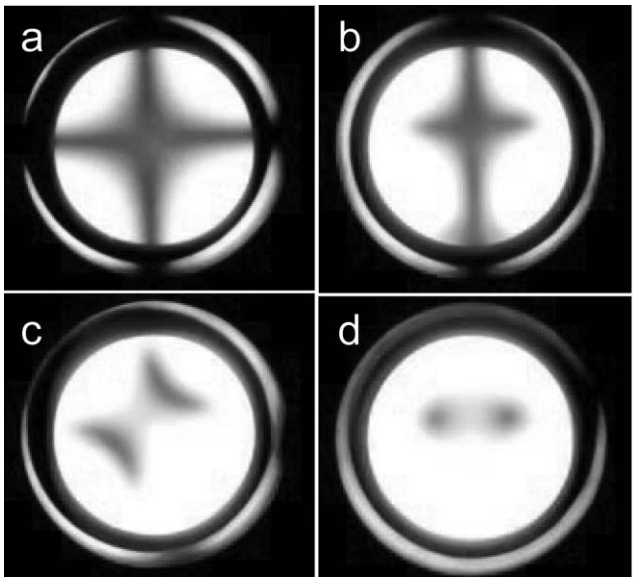

Fig. 4 (a) Conoscopic picture of homeotropically aligned N_u phase of **1c** at 114 °C; (b) asymmetric conoscopic cross in the biaxial nematic phase at 28 °C; (c) sample rotated by 45° with respect to the polariser axis; and (d) conoscopy with circular polarisers inserted above and below the sample, the two dark spots provide a view of the two optic axes of the N_b phase.

suggesting the onset of biaxiality. While the shift in the position of the cross may, in part, be attributable to a slight tilt of the director ***n*** relative to the microscope's optic axis, the change in its shape is entirely due to phase biaxiality. Fig. 4b shows an asymmetric conoscopic cross at 28 °C in the N_b phase. The change in the shape of the cross cannot be caused by mere tilting of nematic director ***n*** of the N_u phase. If only the director ***n*** tilts, then the cross will move off-center but will maintain its symmetric shape of a "plus" sign, which it clearly does not. As the cell is rotated by 45° in between the polarizers, the off-center cross changes to two arcs (isogyres), Fig. 4c. The separation between the two isogyres increases at lower temperatures and is proportional to the degree of biaxiality of the lower temperature N_b phase. A standard technique to visualize the direction of the two optic axes of a biaxial crystal is to place two quarter-wave plates, one before and the second after the sample. Under these conditions, two dark spots are seen, Fig. 4d, which mark the orientations of the two optic axes of the N_b phase and confirm its biaxiality.

The electro-optical response of the homeotropically aligned N_u phase of sample **1c** (Fig. 5a) was investigated at 115 °C. When a square-wave field of 20 *V* and 1 kHz is applied, a Schlieren texture, shown in Fig. 5b, with both, $s = 1$ and ½ disclinations appears immediately as the director ***n*** begins to reorient perpendicular to the field and takes on a planar alignment confirming the negative dielectric nature of these mesogens. However, the texture continues to slowly change and eventually adopt a homogeneous orientation in about two seconds, with ***n*** parallel to the rubbing direction, Fig. 5c. Homogeneous director alignment in the plane of the cell is confirmed by monitoring the transmitted intensity as a function of the angle between *R* and the polarizer axis. One obtains minimum light transmission through the cell when *R* is

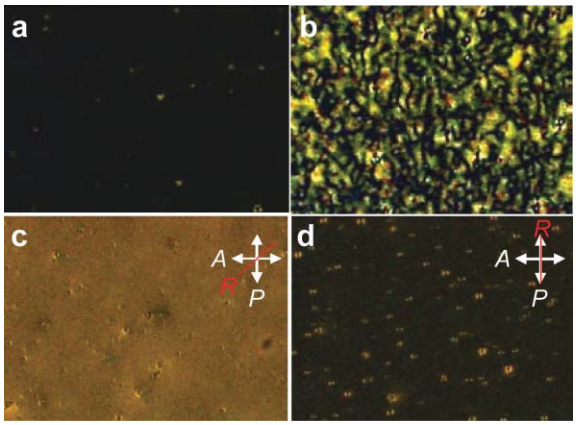

Fig. 5 (a) Homeotropic alignment of the director ***n*** in the N_u phase of sample **1c** at 115 °C with *R* at 45° to the polarizer/analyzer axes and no applied field; (b) a transient Schlieren texture appears with planar orientation of ***n*** when a 2 V μm^{-1} square wave of 1 kHz is applied; (c) stable homogeneous state reached after approx. 2 s with ***n*** in the plane of the substrate. (d) Rotation yields the darkest state when *R* is parallel to the polarizer axis proving that ***n*** orients perpendicular to the field in these dielectrically negative materials.

parallel to either the polarizer or the analyzer axis. At lower temperatures in the N_b phase, the viscosity becomes too large for the applied field to have any effect on the director orientation.

XRD measurements are carried out on both powder and aligned samples[21] filled in glass capillaries of 2 mm diameter (ESI†). In the isotropic phase of compounds **1**, the diffraction pattern consists of two diffuse rings. The inner and outer rings are each composed of two reflections, which are not fully resolved. However, the length scales corresponding to these reflections are estimated to be 22.1, 14.4, 5.1 and 4.2 Å. The presence of four X-ray reflections suggests the biaxial nature of the mesogenic molecules (*cf.* calamitic mesogens possess only two distinct length scales, *i.e.*, the length and lateral dimension of the molecules). The diffraction patterns of samples **1b** and **1c** at 30 °C exhibit four diffuse arcs (Fig. 6a). Two of them are at wide angles; the reflections at 4.6 Å (**1b**) and 4.5 Å (**1c**) are attributed to the mean distance of liquid-like aliphatic chains while the other two, at 3.7 Å (**1b**) and 3.8 Å (**1c**), correspond to the typical mean separation of π-stacks. At small angles, there are also two broad diffuse reflections at 13.9 Å (14.5 Å) and 20.3 Å (21.6 Å) for the two compounds.[22] The diffuse character of all reflections is due to liquid-like positional correlations in the nematic phase which becomes glassy at low temperatures.[23] The temperature dependence of the wide-angle reflections demonstrates decreasing π–π distance at lower temperatures (Fig. 6b). This leads us to conclude that the phenomenon driving the transition from the uniaxial to the biaxial nematic phase is the gradually increasing π-interaction which gives rise to increasing hindrance of molecular rotations about the ***n*** director (see Fig. 1). The fact that the N_u–N_b transition is not observed in conventional DSC scans is consistent with the theoretical prediction of it being second order.

When the sample is cooled into the nematic region in the presence of a magnetic field, the intensity of the small and large angle rings gets concentrated in two pairs of arc

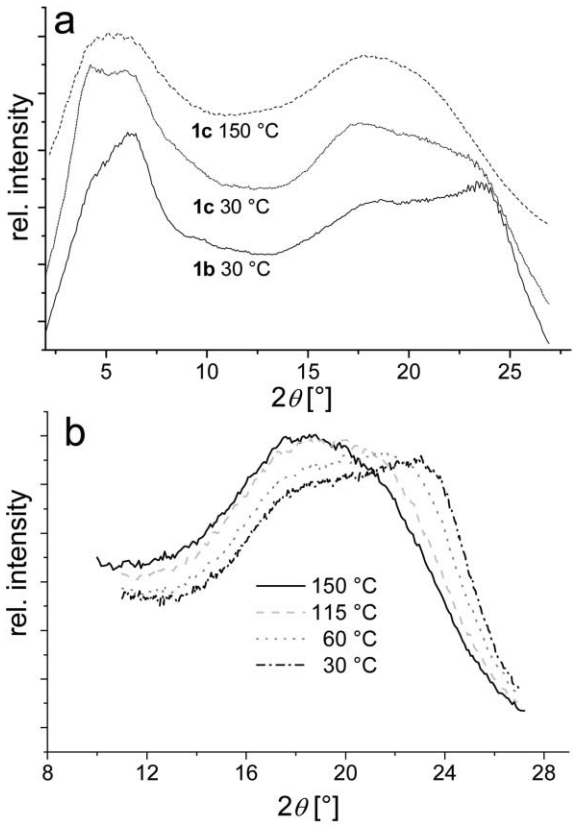

Fig. 6 (a) Powder X-ray diffraction pattern of **1b** and **1c**. (b) Temperature dependent measurements in the wide angle range of **1b**.

reflections (Fig. 7). The inner arcs consist of two reflections in the direction of the magnetic field corresponding to the length scales of 20.3 and 14.3 Å. The separation between these two arcs is not evident at high temperatures but becomes clear upon entering the N_b phase, as seen in Fig. 7 at 71 °C. The two intensity plots in Fig. 7c are obtained by partially masking the diffraction pattern, along orthogonal directions, to best show the splitting. The two outer reflections can now be clearly distinguished. One of these gives rise to X-ray diffraction primarily along the direction perpendicular to the field and, thus, is attributed to director ***n***, while the second weak reflection appears to have no angular concentration of intensity in the plane of the detector. The diffraction angle for this ring can be better estimated *via* an equatorial scan. The large angle reflections correspond to 5.13 and 4.20 Å.

In the small angle region of the diffraction pattern, the two diffuse signals are attributed to intermolecular distances along the bisector of the molecule. Comparison of measured lengths with the molecular dimensions of **1a** shows, that the length scales along the directors ***m*** and ***l*** are larger than the distances calculated from the diffuse peaks in the nematic glass (compare with Fig. 1). This suggests that the molecules are interdigitated. A close inspection of the integrated intensities for **1b** and **1c** shows a more intense second halo at approximately 13.9 Å for the symmetric compound **1b** compared to the non-symmetric **1c** (14.5 Å). The size of the halo at 20.3 Å (21.6 Å) does not change significantly (Fig. 6a), thus the scattered intensity likely arises from periodic electron density which is not affected by the change in the symmetry of the molecule. This could be related to higher electron density in 2,5-dialkoxy substituted aromatic units, which should not differ significantly for **1b** and **1c**. The resulting model, shown in Fig. 8, illustrates essential features inferred from the X-ray patterns of **1b** and **1c**. The aromatic planes are oriented parallel to the surface and the magnetic field *B* (halo at 3.7 Å corresponds to the orientation of director ***n***). In the biaxial phase, additional orientation ordering of the bisector (director ***l***) is obtained. Case **A** shows mesogens (**1c**) where adjacent molecules present different peripheral aromatic units along the bisector

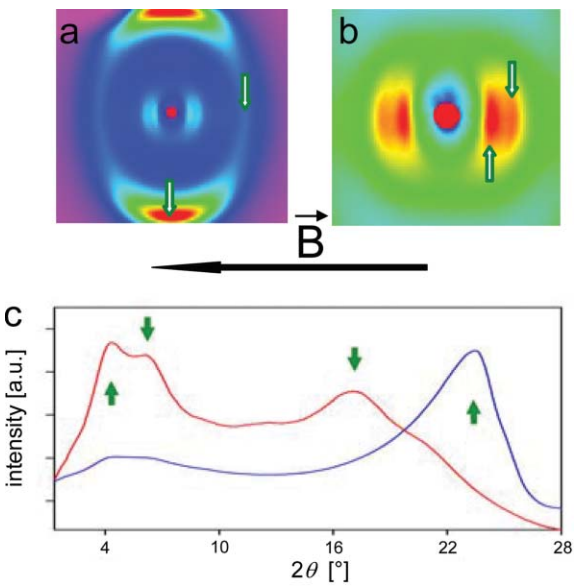

Fig. 7 (a) Diffraction pattern from sample **1c** in the N_b phase 71 °C; (b) Small angle diffraction pattern on expanded scale shows the presence of two reflections; (c) Intensity *vs.* 2θ peaks generated clearly reveal four peaks marked by the arrows.

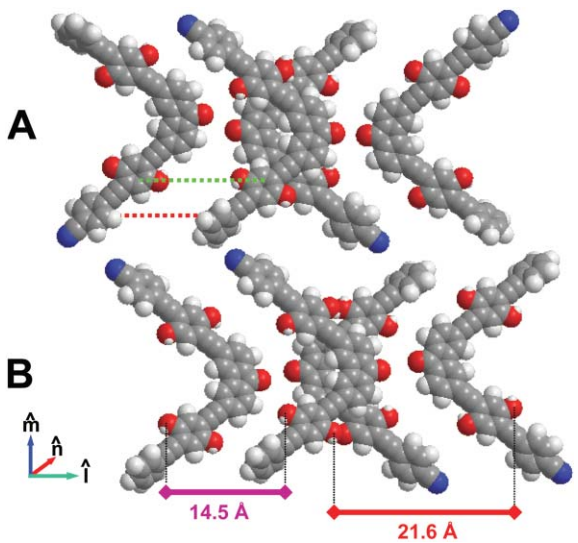

Fig. 8 Model of mean separation of mesogens **1c** in the nematic phase. (A) Cyano-groups of next neighbours, having the carbonyl groups aligned along the same direction of the bisect, pointing to the opposite site and (B) to the same site.

l (anti-parallel alignment of lateral dipoles). No scattering is expected from these molecular parts (red dotted line), whereas the 2,5-dialkoxy substituted aromatic units and the fluorenone centre should still contribute to the peak at 14.5 Å (green dotted line). If all molecules were oriented parallel along the molecular axis *L* and the bisector (case **B**), scattered intensity at 14.5 Å along the orientation direction of the bisector will increase. The latter should always be the case for a symmetric molecule like **1b**, and may be the reason for the relative large halo at approximately 13.9 Å in Fig. 6a. The signal of constant strength at approximately 20.3 or 21.6 Å along the same direction can arise from the symmetrically substituted parts (*i.e.*, the intermediate 2,5-dialkoxy substituted aromatic units) of molecules aligned in an anti-parallel manner, as shown in Fig. 8B for mesogen **1c**.[24]

Summary and conclusions

To summarize, two nematic mesophases are observed exclusively for the mesogens with at least one lateral cyano substituent in the homologous series of rigid nematogens having a fluorenone core with an apex angle of 90°. Although theory predicts uniaxial nematic phases for this value of the apex angle, orthoscopic and conoscopic investigation of the non-symmetric mesogen **1c** clearly indicates a biaxiality at about 40 °C below the clearing point. Results of X-ray diffraction experiments suggest anti-parallel stacking of mesogens along the bisectors and their long axis, as previously proposed for different mesogens in a biaxial SmA phase.[9b] The second order transformation from the uniaxial to biaxial nematic liquid crystal appears to be mediated by increasing π-interaction with decreasing temperature.

Experimental

General methods

Solvents and reagents were purchased from Aldrich and used as received. Column chromatography was performed on silica gel (Merck silica gel 60, mesh size 0.2–0.5 mm). NMR spectra were recorded in $CDCl_3$ on a Bruker Avance 300 with the solvent signal as an internal standard. Mass spectra were recorded on a Finnigan MAT 95 instrument (FD-MS). Elemental analysis was completed in the Microlab of the University of Mainz. Differential scanning calorimetry (DSC) was done on a Mettler Toledo DSC 821 and heating/cooling scans were recorded at 10 °C min^{-1} unless stated otherwise. POM observations were made with a Zeiss Axioscop 40 equipped with a Linkam THMS600 hot stage. Orthoscopy and conoscopy observations were made on cells with a 10–15 μm gap. These were prepared with untreated glass or ITO substrates treated with two different polyimides which are proprietary. One of the polyimides is designed for homeotropic orientation of calamitic liquid crystals. However, the compounds reported here, exhibited opposite alignment, *i.e.*, they aligned in a planar manner. The second rubbed polyimide that aligns calamitic mesogens homogeneously, aligned these materials homogeneously. The electro-optical properties were studied by applying a 1 kHz square wave electric field of variable strength. The melting points reported here were obtained from DSC (onset temperature, first heating) or by POM observations.

X-Ray diffraction (XRD) measurements were carried out on both powder and aligned samples filled in glass capillaries of 2 mm diameter. The samples filled in capillary were aligned by cooling from the isotropic phase to RT in a 0.25 T magnetic field applied perpendicular to the X-ray beam. Other samples were aligned by simple unidirectional shearing and by drawing a fibre from the nematic melt (for results see also Supporting Information†, Fig. S1). Diffraction experiments on sheared and fiber samples were performed using a copper anode (2.2 KW) source with pinhole collimation, an X-ray mirror (Osmic typ CMF15-sCu6), and a Bruker detector (High-star) with 1024 × 1024 pixels. X-Ray patterns were analyzed with the software package Datasqueeze[25] written by Prof. Paul Heiney. Some of the measurements on magnetically aligned samples were performed at the MUCAT's sector of the APS. There, XRD patterns were acquired using a high-resolution (3450 × 3450 pixels) image plate detector MAR-345 (MAR Research) placed at 1158.9 mm from the sample, and λ = 0.7653 Å. The 2-D XRD patterns were analyzed using the software package FIT2D[26] written by A. P. Hammersley of the European Synchrotron Radiation Facility.

Synthesis of 1-bromo-4-iodo-2,5-dimethoxybenzene 2. Compound **2** was synthesised earlier by Hünig *et al.*,[27] however, only a yield as high as 29% has been obtained. Therefore, we used a synthetic strategy analogous to the synthesis reported by Höger *et al.*[13]

1-Bromo-2,5-dimethoxybenzene (9.4 g, 43 mmol), iodine (8.3 g, 33 mmol) and KIO_3 (3.8 g, 18 mmol) were added to a mixture of 50 ml glacial acetic acid, 5 ml sulfuric acid and 12 ml CCl_4 and heated for 5 h to 80 °C. The mixture was poured onto ice and the precipitate was washed with water and methanol. The crude brownish solid was recrystallized from methanol to give 12.4 g (84%) of colourless crystals, mp 142.8 °C (POM; lit.[27] 138 °C). ^{1}H NMR (300 MHz, $CDCl_3$) δ = 3.84, 3.85 (2s, 6H, OCH_3), 7.01, 7.29 (2s, 2H) ppm; ^{13}C NMR (75 MHz, $CDCl_3$) δ = 57.4, 57.5 (OCH_3), 84.4, 112.2 (C_q), 116.3, 123.2 (C_t), 151.2 (C_q), 153.4 (C_q) ppm.

Synthesis of 1-bromo-4-iodohydroquinone 3. The target compound **3** has been published earlier by Höger *et al.*[13] It has been prepared starting from propyloxy derivatives. We developed a synthetic strategy starting from a dimethoxy derivative, since after step two of the reaction path the monobromination product (1-bromo-2,5-dimethoxybenzene) can be easily purified from the dibrominated and non-brominated side products by a simple distillation.

12.0 g (35 mmol) 1-bromo-4-iodo-2,5-dimethoxybenzene dissolved in 140 ml CH_2Cl_2 were cooled to −78 °C. 9.9 ml (105 mmol) BBr_3 in 70 ml CH_2Cl_2 were added to the reaction mixture. Ice was added to the suspension after stirring for 1 h at RT. The precipitate was then filtered and recrystallised from methanol to yield 8.5 g (77%) of a colourless product, mp 165.4 °C (POM) under decomposition (lit.[13] 186 °C). ^{1}H NMR (400 MHz, DMSO-d_6) δ = 7.21, 6.94 (2s, 2H, CH), 9.75, 9.91 (2s br., 2H, CH) ppm; ^{13}C NMR (100 MHz, DMSO-d_6) δ = 83.3, 109.2 (C_q), 117.9, 125.0 (CH, Ar), 147.6, 150.1 (C_q) ppm.

Synthesis of 1-bromo-4-iodo-2,5-dihexyloxybenzene 4. 5.5 g (17.4 mmol) **3** and 3.1 g (47.6 mmol) KOH were dissolved in 100 ml dry DMF and heated to 60 °C. After addition of 8.0 ml (56.7 mmol) *n*-hexylbromide the mixture was stirred for 3 h and poured onto ice. The aqueous layer was extracted with hexane. Evaporation of the solvent yielded white crystals, which were washed with water and ethanol to afford 6.9 g (14.3 mmol, 82%) of a colourless solid, mp 48.5 °C (POM). ^{1}H NMR (400 MHz, $CDCl_3$) δ = 0.90 (t, 3H, CH_3, ^3J = 6.9 Hz), 0.91 (t, 3H, CH_3, ^3J = 6.9 Hz), 1.34 (m, 8H, CH_2), 1.49 (m, 4H, CH_2), 1.79 (m, 4H, CH_2), 3.92 (t, 2H, OCH_2, ^3J = 6.6 Hz), 3.93 (t, 2H, OCH_2, ^3J = 6.6 Hz), 6.98 (s, 1H, CH), 7.27 (s, 1H, CH) ppm; ^{13}C NMR (100 MHz, $CDCl_3$) δ = 14.0 (CH_3), 22.5 (CH_2), 25.5 (CH_2), 29.0 (CH_2), 31.4 (CH_2), 70.2 (OCH_2), 84.7, 112.4 (C_q), 116.9, 117.0 (CH, Ar), 150.3, 152.4 (C_q, C–O) ppm; FT-IR (KBr) ν (cm^{-1}) = 2920, 2856, 1452, 1212; MS (FD) *m*/*z* (%) = 482.1 (100, M^+), 483.1 (20, M + 1), 484.1 (98, M + 2); EA ($C_{18}H_{28}BrIO_2$) calcd C 44.74, H 5.84, found C 44.70, H 5.82%.

Synthesis of 2-[2,5-dihexyloxy-4-(2-phenylethynyl)phenyl]-ethyne 6a. 0.97 g (4.8 mmol) iodobenzene, 60 mg (0.5 mmol) $Pd(PPh_3)_4$ and 25 mg (13.0 mmol) CuI were mixed with 20 ml piperidine. Oxygen was removed by a freeze–pump–thaw procedure and afterwards 1.20 g (2.5 mmol) of **5**[10,14] was added to the stirred reaction mixture. After 12 h the solvent was evaporated, followed by a chromatographic purification (silica, hexane : CH_2Cl_2 = 5 : 1) to yield 1.23 g of the silyl protected derivative of **6a**. The protecting group was cleaved by adding 650 mg (0.0024 mol) $(C_4H_9)_4NF$ to the latter material dissolved in 10 ml THF. After stirring 2 h at RT, the reaction mixture was filtered over florosil. Chromatographic purification (silica, CH_2Cl_2 : hexane 1 : 4) afforded 0.81 g (81%, two steps) of a slightly yellow solid, mp 67.9 °C (POM). ^{1}H NMR (300 MHz, $CDCl_3$) δ = 0.89, 0.91 (2t, 6H, CH_3), 1.35 (m, 4H, CH_2), 1.51 (m, 4H, CH_2), 1.82 (m, 4H, CH_2), 3.34 (s, 1H, CCH), 4.00, 4.01 (2t, 4H, OCH_2), 6.98, 7.00 (2s, 4H, CH), 7.35 (m, 6H, CH), 7.54 (m, 4H, CH) ppm; ^{13}C NMR (75 MHz, $CDCl_3$) δ = 14.0 (CH_3), 22.6, 25.6, 25.7, 29.1, 29.2, 31.5, 31.6 (CH_2), 69.6 (OCH_2), 80.0, 82.2, 85.6, 94.9 (C≡C), 112.5, 114.6 (C_q, Ar), 116.8, 117.8 (CH, Ar), 123.3 (C_q, Ar), 128.3 (CH, Ar), 131.6 (CH, Ar), 153.4, 154.1 (C_q, Ar) ppm; FT-IR (KBr) ν (cm^{-1}) = 3286, 2942, 2853, 1505, 1217; MS (FD) *m*/*z* (%) = 403.2 (100, $[M + H]^+$); EA ($C_{28}H_{34}O_2$) calcd C 83.54, H 8.51, found C 83.55, H 8.58%.

Synthesis of 2-{2,5-dihexyloxy-4-[2-(4-cyanophenyl)-ethynyl]-phenyl}ethyne 6b. 0.75 g (4.1 mmol) 4-bromobenzonitrile, 60 mg (0.5 mmol) $Pd(PPh_3)_4$ and 25 mg (13.0 mmol) CuI were mixed with 15 ml piperidine. Oxygen was removed by a freeze–pump–thaw procedure and afterwards 1.35 g (2.8 mmol) of **5**[10,14] were added to the stirred reaction mixture. After 12 h the solvent was evaporated, followed by a chromatographic purification (silica, hexane : CH_2Cl_2 = 5 : 1) to yield 1.23 g of the silyl protected derivative of **6b**. The protecting group was cleaved by adding 650 mg (0.0024 mol) $(C_4H_9)_4NF$ to a solution of the latter material dissolved in 10 ml THF. After stirring at RT for 2 h, the reaction mixture was filtered over florosil. Chromatographic purification (silica, CH_2Cl_2 : hexane 1 : 2) afforded 0.92 g (77%, two steps) of a slightly yellow solid, mp 97.5 °C (POM). ^{1}H NMR (300 MHz, $CDCl_3$) δ = 0.89, 0.91 (2t, 6H, CH_3), 1.34 (m, 4H, CH_2), 1.51 (m, 4H, CH_2), 1.82 (m, 4H, CH_2), 3.37 (s, 1H, CCH), 3.99, 4.00 (2t, 4H, OCH_2), 6.98, 7.00 (2s, 4H, CH), 7.58, 7.63 (AA′BB′, 6H, CH) ppm; ^{13}C NMR (75 MHz, $CDCl_3$) δ = 14.0 (CH_3), 22.5, 22.6, 25.6, 25.7, 29.1, 29.2, 31.5 (CH_2), 69.5, 69.7 (OCH_2), 82.8, 90.3, 93.0 (C≡C), 111.4, 113.3, 113.7 (C_q, Ar), 116.9, 117.6 (CH, Ar), 118.5 (C_q, Ar) ppm; 131.9, 132.0 (CH, Ar), 153.7, 154.1 (C_q, Ar) ppm; FT-IR (KBr) ν (cm^{-1}) = 3254, 2925, 2855, 2224, 1601, 1221. MS (FD) *m*/*z* (%) = 427.3 (100, M^+); EA ($C_{29}H_{33}NO_2$) calcd C 81.46, H 7.78, N 3.28, found C 81.31, H 7.87, N 3.29%.

Synthesis of 3,6-bis{2-[2,5-dihexyloxy-4-(2-phenylethynyl) phenyl]ethynyl}-9*H*-fluoren-9-one 1a. 79 mg (0.23 mmol) 3,6-dibromo-9*H*-fluoren-9-one, 30 mg $Pd(PPh_3)_4$ and 10 mg CuI were dissolved in 5 ml piperidine. Oxygen was removed by a freeze–pump–thaw procedure and afterwards 200 mg (0.49 mmol) of **6a** was added to the mixture. The reaction was stirred at RT for 12 h. After evaporation of the solvent, the compound was purified by column chromatography (silica, hexane : CH_2Cl_2 = 1 : 1). Yield 100 mg (44%), mp 104.3 °C (DSC data). ^{1}H NMR (300 MHz, $CDCl_3$) δ = 0.91 (m, 12H, CH_3), 1.37 (m, 8H, CH_2), 1.57 (m, 8H, CH_2), 1.88 (m, 8H, CH_2), 4.06 (m, 8H, OCH_2), 7.04, 7.05 (2s, 4H, CH), 7.36 (m, 6H, CH), 7.49 (dd, ABC, ^3J = 7.7 Hz, ^4J = 1.2 Hz, 2H, CH), 7.55 (m, 4H, CH), 7.669 (dd, ABC, ^4J = 1.2 Hz, ^5J = 0.6 Hz, 2H, CH), 7.673 (dd, ABC, ^3J = 7.7 Hz, ^5J = 0.6 Hz, 2H, CH) ppm;[28] ^{13}C NMR (75 MHz, $CDCl_3$) δ = 14.0, 14.1 (CH_3), 22.6, 22.7, 25.7, 25.8, 29.3, 31.6, 31.6, 53.4 (CH_2), 69.6, 69.7 (OCH_2), 85.8, 90.1, 94.3, 95.3 (C_q, C≡C), 113.0, 115.0 (C_q, Ar), 116.8, 117.0, 123.1 (CH, Ar), 123.3 (C_q, Ar), 124.3, 128.3, 128.4 (CH, Ar), 130.0 (C_q, Ar), 131.6, 132.7 (CH, Ar), 133.6, 143.7, 153.6, 153.9 (C_q, Ar), 191.9 (C_q, CO) ppm; FT-IR (KBr) ν (cm^{-1}) = 3054, 2925, 2855, 2200, 1716, 1610, 1599, 1506, 1216, 1026, 917, 876, 851, 782, 753, 689, 668; MS (FD) *m*/*z* (%) = 980.6 (100, M^+); EA ($C_{69}H_{72}O_5$) calcd C 84.45, H 7.40, found C 83.92, H 7.99%.

Synthesis of 3,6-bis(2-{2,5-dihexyloxy-4-[2-(4-cyanophenyl) ethynyl]phenyl}ethynyl)-9*H*-fluoren-9-one 1b. Procedure analogous to the synthesis of **1a**, using **6b** as the ethyne component afforded 118 mg (52%) of an orange solid, melting at 161.3 °C and clearing at 178.1 °C (DSC data).^{1}H NMR (300 MHz, $CDCl_3$) δ = 0.91 (m, 12H, CH_3), 1.38 (m, 8H, CH_2), 1.57 (m, 8H, CH_2), 1.88 (m, 8H, CH_2), 4.06 (m, 8H, OCH_2), 7.03, 7.04 (2s, 4H, CH), 7.49 (dd, ABC, ^3J = 7.7 Hz, ^4J = 1.2 Hz, 2H, CH), 7.60, 7.65 (AA′BB′, 8H, CH), 7.66 (dd, ABC, ^4J = 1.2 Hz, ^5J = 0.6 Hz, 2H, CH), 7.67 (dd, ABC, ^3J = 7.7 Hz, ^5J = 0.6 Hz, 2H, CH) ppm;[28] ^{13}C NMR (75 MHz, $CDCl_3$) δ = 14.0, 14.1 (CH_3), 22.6, 22.7, 25.7, 25.8, 29.2, 31.5, 31.6, 53.4 (CH_2), 69.5, 69.6 (OCH_2), 89.7, 90.3, 93.4, 94.7 (C_q, C≡C), 111.5, 113.6, 114.1 (C_q, Ar), 116.7 (CH, Ar), 118.5 (C_q, CN), 123.1, 124.3 (CH, Ar), 128.2, 129.8 (C_q, Ar), 131.96, 132.0, 132.7 (CH, Ar), 133.7, 143.7, 153.8, 153.9 (C_q, Ar), 191.8 (C_q, CO) ppm; FT-IR (KBr) ν (cm^{-1}) = 3055, 2926, 2855, 2224, 2206, 1708, 1601, 1510, 1217, 1027, 919, 880, 854, 783, 689, 553; MS (FD) *m*/*z* (%) = 1030.4 (100, M^+); EA

($C_{71}H_{70}N_2O_5$) calcd C 82.69, H 6.84, N 2.72, found C 82.59, H 6.77, N 2.63%.

Synthesis of 3-{2-[2,5-dihexyloxy-4-(2-phenylethynyl)phenyl]ethynyl}-6-(2-{2,5-dimethoxy-4-[2-(4-cyanophenyl)-ethynyl]phenyl}ethynyl)-9*H*-fluoren-9-one 1c. Procedure analogous to the synthesis of **1a**, using a 1 : 1 mixture of **6a** and **6b** as the ethyne component afforded 81 mg (33%) of an orange solid, mp 132.3 °C (DSC data). ^{1}H NMR (300 MHz, $CDCl_3$) δ = 0.91 (m, 12H, CH_3), 1.38 (m, 8H, CH_2), 1.57 (m, 8H, CH_2), 1.88 (m, 8H, CH_2), 4.06 (m, 8H, OCH_2), 7.03, 7.05 (2s, 4H, CH), 7.49 (dd, ABC, ^3J = 7.7 Hz, ^4J = 1.2 Hz, 2H, CH), 7.55 (m, 4H, CH), 7.60, 7.65 (AA′BB′, 8H, CH), 7.67 (dd, ABC, ^4J = 1.2 Hz, ^5J = 0.6 Hz, 2H, CH), 7.68 (dd, ABC, ^3J = 7.7 Hz, ^5J = 0.6 Hz, 2H, CH) ppm;[28] ^{13}C NMR (75 MHz, $CDCl_3$) δ = 14.0, 14.1 (CH_3), 22.6, 22.7, 25.7, 25.8, 29.2, 31.5, 31.6, 53.4 (CH_2), 69.5, 69.6, 69.7 (OCH_2), 85.5, 89.7, 90.1, 90.4, 93.4, 94.3, 94.7, 95.3 (C_q, C≡C), 111.4, 112.9, 113.5, 114.1, 115.0 (C_q, Ar), 116.8, 117.0 (CH, Ar), 118.5 (C_q, CN), 123.1 (CH, Ar), 123.3 (C_q, Ar), 124.3, 128.3, 128.4 (CH, Ar), 129.8, 130.0 (C_q, Ar), 131.6, 131.9, 132.0, 132.7 (CH, Ar), 133.5, 133.7, 143.66, 143.71, 153.6, 153.8, 153.9 (C_q, Ar), 191.8 (C_q, CO) ppm; FT-IR (KBr) ν (cm^{-1}) = 3057, 2929, 2858, 2223, 2207, 1708, 1601, 1508, 1218, 1028, 919, 881, 853, 838, 783, 754, 690, 670, 554; MS (FD) *m*/*z* (%) = 1005.8 (100, M^+); EA ($C_{70}H_{71}NO_5$) calcd C 83.55, H 7.11, N 1.39, found C 83.58, H 7.37, N 1.31%.

Acknowledgements

We are grateful to the Communauté Francaise de Belgique (ARC n° 00/05-257), the Bundesministerium für Bildung und Forschung (BMBF) and to the US National Science Foundation (grant DMR-03-12792) for their financial support. We thank Prof. Herbert Meier for making the FD mass and elemental analysis at the University of Mainz available to us and to Prof. Yves Geerts for support and helpful discussions. We are grateful to Michael Bach and Prof. Jochen Gutmann for their help during X-ray measurements at the Max Planck Institute for Polymer Research at Mainz. We thank Dr N. E. Zafeiropoulos at the Institute for Polymer Research Dresden for the help with additional X-ray measurements and fruitful discussions. Use of the Advanced Photon Source (APS) was supported by the U.S. Department of Energy (DOE), Basic Energy Sciences (BES), Office of Science, under Contract No. W-31-109-Eng-38. The Midwestern Universities Collaborative Access Team's (MUCAT) sector at the APS is supported by the U.S. DOE, BES, Office of Science, through the Ames Laboratory under Contract No. W-7405-Eng-82. Any opinions, findings, and conclusions or recommendations expressed in this publication are those of the author(s) and do not necessarily reflect the views of the National Science Foundation.

References

1 (*a*) B. R. Acharya and S. Kumar, *Bull. Am. Phys. Soc.*, 2000, **45**, 101; (*b*) B. R. Acharya, A. Primak, T. J. Dingemans, E. T. Samulski and S. Kumar, *Pramana*, 2003, **61**, 231; (*c*) B. R. Acharya, A. Primak and S. Kumar, *Phys. Rev. Lett.*, 2004, **92**, 145506; (*d*) L. A. Madsen, T. J. Dingemans, M. Nakata and E. T. Samulski, *Phys. Rev. Lett.*, 2004, **92**, 145505.

2 M. J. Freiser, *Phys. Rev. Lett.*, 1970, **24**, 1041.

3 L. J. Yu and A. Saupe, *Phys. Rev. Lett.*, 1980, **45**, 1000.

4 (*a*) G. R. Luckhurst, *Thin Solid Films*, 2001, **393**, 40; (*b*) K. Praefcke, *Braz. J. Phys.*, 2002, **32**, 564.

5 (*a*) R. Alben, *Phys. Rev. Lett.*, 1973, **30**, 778; (*b*) R. Alben, *J. Chem. Phys.*, 1973, **59**, 4299; (*c*) J. P. Straley, *Phys. Rev.*, 1974, **A10**, 1881; (*d*) H. H. Wensink, G. J. Vroege and H. N. W. Lekkerkerker, *Phys. Rev.*, 2002, **E66**, 041704.

6 (*a*) P. J. Champ, M. P. Allen and A. J. Masters, *J. Chem. Phys.*, 1999, **111**, 9871; (*b*) P. I. C. Teixeira, A. J. Masters and B. M. Mulder, *Mol. Cryst. Liq. Cryst.*, 1999, **323**, 167.

7 V. Prasad, S.-W. Kang, K. A. Suresh, L. Joshi, Q. Wang and S. Kumar, *J. Am. Chem. Soc.*, 2005, **127**, 17224.

8 (*a*) G. R. Luckhurst, *Angew. Chem.*, 2005, **117**, 2894, (*Angew. Chem., Int. Ed.*, 2005, **44**, 2834); (*b*) G. R. Luckhurst, *Nature*, 2004, **430**, 413.

9 (*a*) R. A. Reddy and B. K. Sadashiva, *J. Mater. Chem.*, 2004, **14**, 310; (*b*) B. K. Sadashiva, R. A. Reddy, R. Pratibha and N. V. Madhusudana, *J. Mater. Chem.*, 2002, **12**, 943; (*c*) B. K. Sadashiva, R. A. Reddy, R. Pratibha and N. V. Madhusudana, *Chem. Commun.*, 2001, 2140.

10 M. Lehmann and J. Levin, *Mol. Cryst. Liq. Cryst.*, 2004, **411**, 273.

11 H. Meier, M. Lehmann, H. C. Holst and D. Schwöppe, *Tetrahedron*, 2004, **60**, 6881.

12 (*a*) Z. Bao, Y. Chen, R. Cai and L. Yu, *Macromolecules*, 1993, **26**, 5281; (*b*) S. H. Chen, A. C. Su, S. R. Han, S. A. Chen and Y. Z. Lee, *Macromolecules*, 2004, **37**, 181.

13 S. Höger, K. Bonrad, G. Schäfer and V. Enkelmann, *Z. Naturforsch., B: Chem. Sci.*, 1998, **53b**, 960. In contrast to the reference compound **3** was obtained from dimethyl ether **2** as the starting material.

14 S. Höger, K. Bonrad, A. Mourran, U. Beginn and M. Möller, *J. Am. Chem. Soc.*, 2001, **123**, 5651.

15 J. Ipatschki, R. Hosseinzadeh, P. Schlaf, E. Dreiseidler and R. Goddard, *Helv. Chim. Acta*, 1998, **81**, 1821.

16 Crystal data: $C_{69}H_{72}O_5$, M = 981.27, monoclinic, *C*2/*c*, a = 16.0034(9) Å, b = 33.0383(7) Å, c = 10.6224(5) Å, β = 97.142(2)°, V = 5572.8(4) Å^3, z = 4, $\rho_{calc.}$ = 1.42 g cm^{-3}, crystal size 0.1 × 0.2 × 1.0 mm^3, Cu-Kα radiation λ = 1.54178 Å, μ = 0.558 mm^{-1}, scan type: $\omega/2\theta$, scan range: 2 < θ < 74°, T = 193 K, 6052 reflections measured, 5636 unique, Lp – correction, 5636 reflections refined, R_{int} = 0.0269, structure solution with direct methods (program SIR97[29]), refinement against F^2 using full matrix least square refinement (program SHELXL97[30]), 358 refined parameters, w*R*2 = 0.1207, *R*1 (for 4561 refl. $|F|/\sigma(F) > 4$) = 0.0453, hydrogen atom at calculated positions and refined using riding motion model with isotropic displacement parameters, peaks in final differential Fourier calculation: 0.27, −0.18 e Å^{-3}. CCDC reference number 294987. For crystallographic data in CIF or other electronic format see DOI: 10.1039/b605718g.

17 For the estimation of dipole moments, the experimental values for fluorenone 3.38 D (D. A. Pitt and C. P. Smyth, *J. Am. Chem. Soc.*, 1959, **80**, 1061) and benzonitrile 4.05 D (K. B. Everard, L. Kumar and L. E. Sutton, *J. Chem. Soc.*, 1951, 2807) in benzene were used.

18 K. Praefcke, *Mol. Cryst. Liq. Cryst.*, 2001, **364**, 15.

19 Y. Galerne, *Mol. Cryst. Liq. Cryst.*, 1998, **323**, 211.

20 Surface effects may induce phase biaxiality. However, it was suggested that in thick films such influence should be vanishingly small (B. K. Sadashiva, personal communication). The films investigated had a thickness of 10–20 μm.

21 Samples were aligned in a magnetic field of 0.25 T, perpendicular to the X-ray beam. Slow cooling of the material in a strong magnetic field (7 T) induced a crystallisation process, due to the metastable nature of the monotropic nematic phase of **1c** and the supercooled nematic phase of **1b**.

22 These *d* values can be compared with distances found in the crystal structure of **1a**. For more details see the Supporting Information†.

23 Correlation lengths have been estimated from the half-width of the signals for **1b**: 47.5 Å (2.3 molecules (≅20.3 Å)); 75.5 Å (≅5.4 molecules (13.9 Å)); 12.2 Å (≅2.6 CH_2 (4.7 Å)); 40.6 Å (≅11.0 molecules (3.7 Å)). For **1c**: 84.9 Å (≅3.9 molecules (21.6 Å)); 58.9 Å (≅4.1 molecules (14.5 Å)); 13.2 Å (≅2.9 CH_2 (4.5 Å)); 40.1 Å (≅10.6 molecules (3.8 Å)).

24 Another explanation for the observed X-ray pattern may include a model where different biaxial domains align with their director **n** or director **m** perpendicular to the X-ray beam, *i.e.* parallel to the magnetic field. A similar pattern has already been observed by Diele *et al.*: K. Praefke, B. Kohne, B. Gundogan, D. Demus, S. Diele and G. Pelzl, *Mol. Cryst. Liq. Cryst. Lett. Sect.*, 1990, **7**, 27.
25 P. Heiney, *Datasqueeze 2.0.7*, Datasqueeze software, Wayne, PA, USA, 2006.
26 A. P. Hammersley, *Fit2d version 12.040*, ESRF, Grenoble, France, 2006.
27 S. Hünig, R. Bau, M. Kemmer, H. Meixner, T. Metzenthin, K. Peters, K. Sinzger and J. Gulbis, *Eur. J. Org. Chem.*, 1998, 335–348.
28 Coupling constants and chemical shifts of the ABC system were obtained by the best fit of the ABC pattern using the program MestRe–C 2.3a.
29 A. Altomare, M. C. Burla, M. Camalli, G. L. Cascarano, C. Giacovazzo, A. Guagliardi, A. G. G. Moliterni, G. Polidori and R. Spagna, *J. Appl. Crystallogr.*, 1999, **32**, 115.
30 G. M. Sheldrick, *SHELXL-97, Program for refinement of crystal structures*, University of Göttingen, Germany, 1997.